OFDM-based analog multiband: a scalable design for indoor mm-wave wireless communication

Hossein Roufarshbaf
Dept. of Electrical and Computer Eng.
University of California, Santa Barbara
Email: hroufarshbaf@ece.ucsb.edu

Upamanyu Madhow
Dept. of Electrical and Computer Eng.
University of California, Santa Barbara
Email: madhow@ece.ucsb.edu

Sridhar Rajagopal
Samsung Research America
Dallas, TX
Email: sridhar.r@samsung.com

***Abstract*—We propose an approach to scaling communication bandwidths over dispersive channels that preserves the advantage of DSP-centric receiver design, while sidestepping the difficulty of scaling analog-to-digital conversion (ADC) to higher and higher bandwidths. This is accomplished by channelizing the available bandwidth into contiguous subbands in the analog domain, with the width of a subband chosen so that digitization is possible at reasonable cost and power using existing ADC technology. We illustrate these ideas for multiGigabit indoor mm-wave communication, with GHz bandwidth divided into subbands of width 250-500 MHz. The channel delay spread even after beamforming can be as large as 20 ns, hence the channel seen within subbands is dispersive. Further, the contiguity of subbands and the sloppy analog channelization implies that adjacent subbands interfere with each other. We show that OFDM within subbands is an attractive approach in these settings: the channel dispersion within subbands can be handled with a moderate cyclic prefix, while the inter-band interference manifests itself only on the edge subcarriers. We clarify the structure of the inter-band interference, and show that it is effectively suppressed by adaptive linear Minimum Mean Squared Error (MMSE) techniques for joint detection across adjacent subbands. Our performance evaluation is carried out using channel models developed for the IEEE 802.11ad 60 GHz standard.**

I. Introduction

Millimeter wave communication offers the opportunity of scaling wireless bandwidths and data rates by orders of magnitude, to multiples of GHz (e.g., the 60 GHz band has 7 GHz of unlicensed spectrum). In utilizing such large bandwidths, we would still like to enjoy the economies of scale provided by Moore's law that have driven mass market WiFi and cellular technologies, with transceivers that utilize digital signal processing (DSP) to the greatest extent possible. However, the cost and power of analog-to-digital converters scale poorly with signal bandwidth [1]. Thus, a natural idea is to break the available bandwidth into subbands which can be discretized separately by ADCs of "reasonable" speed, as determined by current technology. A key challenge, of course, is the inter-band interference that results from imperfect analog channelization, as we do not wish to sacrifice bandwidth efficiency by putting in large guard bands. However, since we are able to digitize each subband, it becomes possible to use DSP techniques to handle such interference, as well as standard impairments such as channel dispersion within a subband. In this paper, we explore such design issues in the context of an indoor mm-wave communication channel, using OFDM within subbands to handle channel dispersion.

Contributions: Our key contributions are as follows. Starting from indoor 60 GHz channel models developed during the IEEE 802.11ad standardization process, we model the channels seen by individual subbands, assuming that the transmitter and receiver form beams along a dominant ray. We show that, even for such beamformed links, the residual channel dispersion within a subband of 250-500 MHz width is still several signal samples long. Focusing on OFDM as a well-understood DSP-centric approach to handle such dispersion, we then investigate the structure of inter-band interference for a system in which there is no guard band between subbands. As expected, we find that only the edge subcarriers in a subband encounter interference from adjacent subbands. More interestingly, we find that the nth subcarrier in a given subband encounters interference only from the nth subcarriers in the adjacent subbands to the left and right. Furthermore, linear MMSE adaptation applied on an observation vector obtained by grouping the frequency domain samples for subcarrier n from adjacent subbands is effective in suppressing inter-band interference. We provide numerical results based on IEEE 802.11ad channel models.

Related work: Analog multiband transmission was proposed many decades ago, but then was rendered obsolete by OFDM. It has been recently considered for wired backplane channels [2], [3], but large guard bands are used to avoid inter-band interference. Analog multiband techniques have also been considered for an indoor 60 GHz channel [4], but a guard band is implicitly provided by stacking the subbands next to each other *after* accounting for excess bandwidth, and channel dispersion was not addressed. The application of analog multiband to *outdoor* 60 GHz channels was considered in [5] (the approach was termed analog multitone in that paper). Like the present paper, no guard band was used, and DSP techniques were used to handle both channel dispersion and inter-band interference. However, single carrier modulation was used within each subband, hence the structure of the DSP for interference suppression was different. The delay spread for the longer range line-of-sight (LOS) outdoor links in [5] was smaller than in our indoor setting, where it can be as large as 20 ns even after beamforming along the dominant ray, which might be non line-of-sight (NLOS).

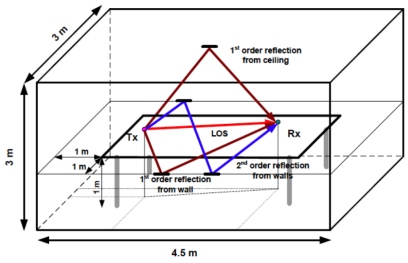

Fig. 1. The conference room scenario used for standard modeling of the indoor mm-wave channel [6].

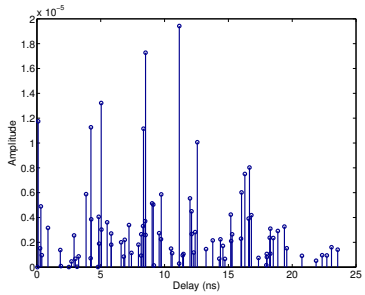

Fig. 2. A realization of the channel amplitude vs. delay for the conference room scenario.

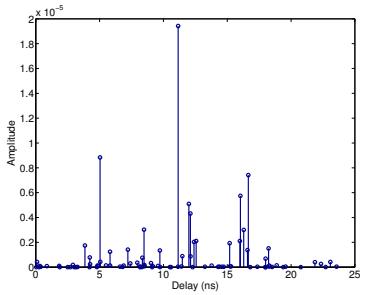

Fig. 3. The channel realization in Figure 2, beamformed toward the strongest path.

$$h(t,\phi_{tx},\theta_{tx},\phi_{rx},\theta_{rx}) = \sum_i A^{(i)} C^{(i)}(t-T^{(i)},\phi_{tx}-\Phi_{tx}^{(i)},\theta_{tx}-\Theta_{tx}^{(i)},\phi_{rx}-\Phi_{rx}^{(i)},\theta_{rx}-\Theta_{rx}^{(i)}), \quad (1)$$

$$C^{(i)}(t,\phi_{tx},\theta_{tx},\phi_{rx},\theta_{rx}) = \sum_k \alpha^{(i,k)}\delta(t-\tau^{(i,k)})\delta(\phi_{tx}-\phi_{tx}^{(i,k)})\delta(\theta_{tx}-\theta_{tx}^{(i,k)})\delta(\phi_{rx}-\phi_{rx}^{(i,k)})\delta(\theta_{rx}-\theta_{rx}^{(i,k)}). \quad (2)$$

This paper is organized as follows: we first review the mm-wave indoor communication channel model used in this paper (Section II). The proposed transceiver architecture is discussed in Section III. In Section IV, we describe the structure of the inter-band interference in terms of its effect on each OFDM subcarrier, and in Section V, we describe our approach to interference suppression. Simulation results and conclusions are provided in Sections VI and VII, respectively.

II. Indoor mm-wave Wireless Channel

In the context of the IEEE 802.11ad standard, significant effort has been devoted to modeling the indoor mm-wave wireless channel, based on ray tracing simulations and experimental measurements [6], [7]. This standard model draws on the quasi-optical nature of the mm-wave signal to model the channel based on a small number of paths (LOS and reflections), with each reflected path modeled as a cluster of closely spaced rays [8]. The channel impulse response is modeled as in (1) and (2), where $A^{(i)}$ is a 2×2 matrix gain of the i-th cluster that presents polarization characteristics, $C^{(i)}$ shows the channel impulse response for cluster i, δ is the Dirac delta function, $T^{(i)}$, $\Phi_{tx}^{(i)}$, $\Theta_{tx}^{(i)}$, $\Phi_{rx}^{(i)}$, $\Theta_{rx}^{(i)}$ are the time and angular characteristics of the cluster that are termed inter-cluster parameters, and $\alpha^{(i,k)}$, $\tau^{(i,k)}$, $\phi_{tx}^{(i,k)}$, $\theta_{tx}^{(i,k)}$, $\phi_{rx}^{(i,k)}$, $\theta_{rx}^{(i,k)}$ are the amplitude, time, and angular characteristics of the k-th ray in i-th cluster that are termed intra-cluster parameters.

The statistical distributions for the inter-cluster and the intra-cluster parameters are given for various indoor scenarios such as the conference room, living room, and cubicle office [6]. Figure 1 shows the conference room scenario where two stations are located on the conference room desk. The LOS path, the 1st order reflected paths, and the 2nd order reflected paths are plotted for this scenario. A realization of the channel impulse response, assuming that the LOS path is blocked, is plotted in Figure 2. The delay spread of the simulated channel impulse response is 25 ns that represents a dispersive channel within the subbands. We assume that the transmitter and receiver are each equipped with 4×4 square arrays $\lambda/2$ element spacing (one of the advantages of the small wavelength is that such arrays can be realized with compact form factor), and that these are both steered towards the strongest path. The beamformed channel for the realization we have considered is shown in Figure 3. While the channel is more concentrated, we observe that the delay spread is still large (12 ns) even after beamforming.

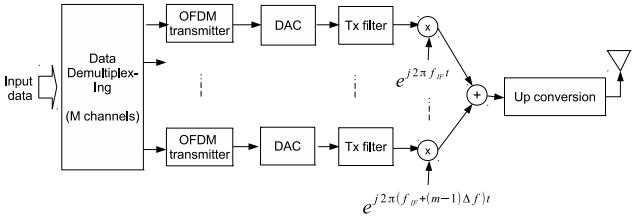

Fig. 4. Analog multiband structure at the transmit side.

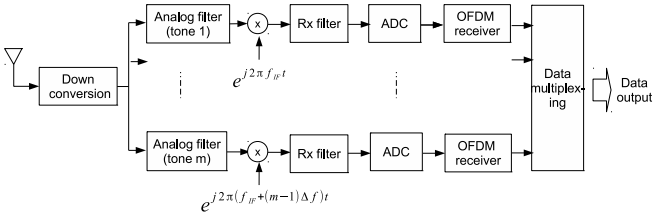

Fig. 5. Analog multiband structure at the receive side.

III. Multiband Architecture

The purpose of the analog multiband structure is to break the available bandwidth (e.g. MF_s Hz) into multiple parallel subbands (M subbands), each discretized by an ADC of reasonable speed (F_s Hz). As we observed in Section II, the channel delay spread is significant even after beamforming, so that OFDM is an attractive signaling technique for equalization within each subband. Figure 4 shows the transmitter

side of the analog multiband architecture. The transmit data is demultiplexed into M parallel subbands. Data over each subband is modulated through the OFDM transmitter block. The digital to analog converter (DAC) blocks and the transmit filters stack up the subbands at intermediate frequency (IF) in the analog domain, spaced at Δf: we assume that guard bands are not used, hence $\Delta f = F_s$, the sampling rate within each subband. The IF analog signal is upconverted to the carrier frequency band and transmitted over the directional communication channel.

At the receiver (Figure 5), the received signal is downconverted to IF, then demultiplexed using a set of parallel analog receive filters, each tuned to pass the associated subband signal. The received signal on each subband is downconverted to baseband and discretized using ADCs. These parallel discretized signals are demodulated at the OFDM receivers (which, as we shall see, do need to be coupled lightly in order to suppress inter-band interference) and are multiplexed to form the received data stream.

IV. Interference Structure

Suppose that the input data stream is demultiplexed into M subbands. The OFDM transmitter for each subband works at a sampling rate of F_s Hz and contains N subcarriers. The OFDM data stream for subband m is denoted by

$$\mathbf{b}_k^{(m)} = [b_{k,1}^{(m)}, \cdots, b_{k,N}^{(m)}], \tag{3}$$

where k denotes OFDM symbol index. After taking the inverse discrete Fourier transform (IDFT) and adding the cyclic prefix, the time domain samples for the OFDM transmitted symbol are denoted by $\mathbf{B}_k^{(m)}$. As discussed before, we consider a guard band free channelizing scheme to use all available spectrum. Therefore, we expect that the neighbor subbands signals (subbands $m-1$ and $m+1$) interfere with the current subband due to non-ideal transmit and receive filters used in analog channelization. Once we include inter-band interference (we assume this is restricted to the two adjacent bands), the received signal of subband m after analog to digital conversion is modeled as

$$\begin{aligned}\mathbf{r}_k^{(m)} &= \mathbf{h}^{(m)} \circledast \mathbf{B}_k^{(m)} \\ &\quad + \mathbf{h}^{(m-)} \circledast \mathbf{B}_k^{(m-1)} + \mathbf{h}^{(m+)} \circledast \mathbf{B}_k^{(m+1)} + \mathbf{w}_k^{(m)},\end{aligned} \tag{4}$$

where $\circledast$ denotes the circular convolution, $\mathbf{h}^{(m)}$ is the impulse response of the equivalent channel impulse response for subband m, $\mathbf{h}^{(m-)}$ is the impulse response of the equivalent interfering channel from subband $m-1$, $\mathbf{h}^{(m+)}$ is the equivalent interfering channel from subband $m+1$, and $\mathbf{w}_k^{(m)}$ is the additive white Gaussian noise. We have assumed here that the OFDM transmitted symbols over parallel subbands are synchronized in time and have the same length of cyclic prefix. With these assumptions, the circular convolution operation in (4) is valid for the interfering subbands as well. The equivalent channel impulse response for subband m and interfering subbands are related to the standard mm-wave channel impulse response (1) at the subband symbol rate through

$$\mathbf{h}^{(m)} = p_{Tx} * h * p_{Rx} \tag{5}$$

$$\mathbf{h}^{(m-)} = (p_{Tx} e^{j2\pi\Delta f t}) * h * p_{Rx} \tag{6}$$

$$\mathbf{h}^{(m+)} = (p_{Tx} e^{-j2\pi\Delta f t}) * h * p_{Rx}, \tag{7}$$

where $*$ denotes the convolution operation and p_{Tx} and p_{Rx} denote the impulse response of the transmit and receive filters (Figures 4 and 5), respectively. Within the OFDM symbol, the received samples after removing the cyclic prefix and taking the discrete Fourier transform (DFT) are given by

$$\begin{aligned}\mathbf{R}_k^{(m)} &= \mathbf{H}^{(m)} .* \mathbf{b}_k^{(m)} \\ &\quad + \mathbf{H}^{(m-)} .* \mathbf{b}_k^{(m-1)} + \mathbf{H}^{(m+)} .* \mathbf{b}_k^{(m+1)} + \mathbf{W}_k^{(m)},\end{aligned} \tag{8}$$

where $.*$ denotes element by element multiplication of two vectors, $\mathbf{H}^{(m)}$ is the DFT of the equivalent transmit channel, and $\mathbf{H}^{(m-)}$ and $\mathbf{H}^{(m+)}$ denote the DFT of the equivalent interfering channels. We observe that, by virtue of the cyclic prefix, the interference seen by OFDM symbol k is only due to OFDM symbol k from each of the neighboring subbands. We can therefore restrict attention to one OFDM symbol at a time, and drop the index k from our notation. Rewriting (8) for OFDM subcarrier n, the received signal is given by

$$\begin{aligned}R_n^{(m)} &= H_n^{(m)} . b_n^{(m)} + H_n^{(m-)} . b_n^{(m-1)} \\ &\quad + H_n^{(m+)} . b_n^{(m+1)} + W_n^{(m)} .\end{aligned} \tag{9}$$

The preceding interference model shows that subcarrier n encounters interference only from subcarrier n of the adjacent subbands. Hence, the interference across subbands can be handled by joint detection for each subcarrier over all subbands. The received signal on subcarrier n of all the subbands is modeled as

$$\mathbf{R}_n = \mathcal{H}_n \mathbf{b}_n + \mathbf{w}_n, \tag{10}$$

where

$$\mathbf{R}_n = [R_n^{(1)}, R_n^{(2)}, \cdots, R_n^{(M)}]^T, \tag{11}$$

$$\mathbf{b}_n = [b_n^{(1)}, b_n^{(2)}, \cdots, b_n^{(M)}]^T, \tag{12}$$

$$\mathbf{w}_n = [W_n^{(1)}, W_n^{(2)}, \cdots, W_n^{(M)}]^T, \text{ and} \tag{13}$$

$$\mathcal{H}_n = \begin{bmatrix} H_n^{(1)} & H_n^{(1+)} & 0 & \cdot & 0 \\ H_n^{(2-)} & H_n^{(2)} & H_n^{(2+)} & \cdots & 0 \\ 0 & H_n^{(3-)} & H_n^{(3)} & \cdots & 0 \\ \vdots & & & & \\ 0 & 0 & 0 & \cdots & H_n^{(M)} \end{bmatrix}. \tag{14}$$

Data transmitted on subcarrier n can now be jointly detected across subbands using the model (10). For M parallel subbands and N subcarriers per subband, the maximum number of non-zero channel coefficients is $N \times (3M-2)$. Of course, we expect inter-band interference to be significant only at the edges of the subbands, hence the effort on interference suppression need only be expended on edge subcarriers, as discussed in more detail in the next section.

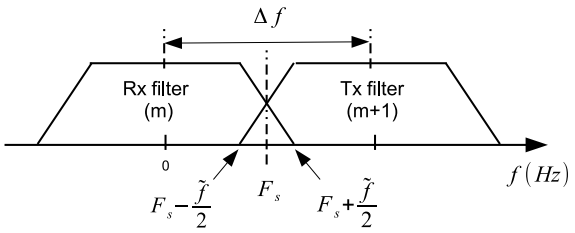

Fig. 6. Baseband equivalent model for subband m and the interfering subband $m+1$

A. Variation across subcarriers

From (9), we find that the n-th subcarrier in a given subband encounters interference only from the n-th subcarrier of the adjacent subbands. inter-band interference occurs since, once we account for the frequency separation between subbands, the analog transmit filter for subband $m \pm 1$ and the receive filter for subband m overlap only in their transition bands. Therefore, we expect that the subcarriers at the edges encounter more interference than those in the middle of the subband. In order to develop more specific insight, consider the baseband equivalent model for the interference due to subband $m+1$ seen by subband m (the interference due to subband $m-1$ follows an entirely analogous pattern).

Following (4), the coefficients of the effective interfering channel discrete Fourier transform (DFT) with size N, i.e. $\mathbf{H}^{m+}$, determines the amount of interference for each subcarrier. The effective interfering channel impulse response is defined in (7). The frequency response of the effective interfering channel is the product of the frequency responses of the receive filter (subband m), transmission channel h, and the transmit filter (subband $m+1$). Figure 6 shows the frequency response of the receive filter for subband m and the transmit filter for subband $m+1$. The continuous time Fourier transform (CTFT) of the effective interfering subband ($Hc^{(m+)}$) is approximately zero except for the overlapping region

$$\begin{cases} Hc^{(m+)}(f) \approx 0 & \text{for } f < F_s - \tilde{f}/2 \\ Hc^{(m+)}(f) \neq 0 & \text{for } F_s - \tilde{f}/2 < f < F_s + \tilde{f}/2 \end{cases}, \quad (15)$$

where $\tilde{f}$ denotes the amount of frequency overlap between subbands m and $m+1$. The frequency response of the sampled effective channel ($Hs^{(m+)}$) is related to the continuous time Fourier transform (CTFT) of the channel through aliasing:

$$Hs^{(m+)}(f) = F_s \sum_{l=-\infty}^{+\infty} Hc^{(m+)}(f - lF_s). \quad (16)$$

The discrete Fourier transform (DFT) with length N is derived by taking samples from one period of the sampled CFTF (16) at the sampling rate of N/F_s

$$\begin{aligned} H_n^{(m+)} &= Hs^{(m+)}(nF_s/N) \quad (17) \\ &= \sum_{k=-\infty}^{+\infty} Hs^{(m+)}\left(\frac{nF_s}{N} - kF_s\right) \quad \text{for } n = 0, \cdots, N-1. \end{aligned}$$

Using (15) and (17), the DFT coefficients of the interfering channel are

$$\begin{cases} H_n^{(m+)} \neq 0 & \text{for } 0 \leq n < \frac{\tilde{f}N}{2F_s} \\ H_n^{(m+)} \neq 0 & \text{for } N - \frac{\tilde{f}N}{2F_s} \leq n < N \\ H_n^{(m+)} \approx 0 & \text{elsewhere} \end{cases}. \quad (18)$$

We observe that, due to aliasing, the effective interference from subband $m+1$ hits the OFDM subcarriers in subband m on both the left and right boundaries. Analogously, the interference from subband $m-1$ also hits the OFDM subcarriers on both boundaries. However, the middle subcarriers do not see interference (under reasonable assumptions on filter transition bands), hence the channel matrix (14) is diagonal for them. Thus, the receiver needs to perform joint data detection, or interference suppression, only for boundary subcarriers.

V. Interference Suppression

We investigate two linear channel equalization scenarios for joint detection of the boundary subcarriers. In the first scenario, we assume that the channel is perfectly known and we use a zero-forcing linear channel equalizer. In the second scenario, we consider a MMSE linear equalizer implemented using least squares adaptation based on a training sequence.

a) Zero-Forcing Linear Equalizer: Assuming that the channel matrix for each subcarrier ($\mathcal{H}_n$) is known at the receiver, a zero-forcing (ZF) linear equalizer for each OFDM subcarrier can be applied for joint detection of the transmitting symbols over the subbands. For the interference model (10), the ZF linear equalizer jointly estimates the symbols of subcarrier n through

$$\hat{\mathbf{b}}_n = \mathcal{H}_n^{-1}\mathbf{R}_n. \quad (19)$$

The ZF equalizer incurs noise enhancement, but based on the per-subcarrier interference model (10) and (14), we expect this to be significant only for the boundary subcarriers.

b) MMSE Linear Equalizer: The ZF equalizer requires explicit channel estimates, whereas the MMSE equalizer can be implemented adaptively based on a training sequence. The estimated symbols are related to the received symbols for each subcarrier through

$$\hat{\mathbf{b}}_n = \mathbf{C}_n^H \mathbf{R}_n, \quad (20)$$

where ^{H} denotes matrix Hermitian operation, and $\mathbf{C}_n$ is the equalizer matrix, chosen to minimize the mean squared error (MSE) given by

$$\min_C \mathbf{E}\{(\mathbf{b}_n - \hat{\mathbf{b}}_n)^2\}, \quad (21)$$

where $\mathbf{E}\{.\}$ denotes the expectation operation. Substituting (20) into (21) and minimizing the mean square error by taking the derivative with respect to matrix $\mathbf{C}$, we get the standard solution:

$$\mathbf{C}_n = \mathcal{R}^{-1}\mathcal{P}, \quad (22)$$

TABLE I
OFDM PARAMETERS USED IN SIMULATIONS.

OFDM symbol rate	Number of subcarriers	Subcarrier spacing	CP length	Modulation scheme
256 MHz	64	4 MHz	16	16-QAM

where $\mathcal{R} = \mathbf{E}\{\mathbf{R}_n\mathbf{R}_n^H\}$ is the correlation matrix of the observations and the cross correlation matrix

$$\mathcal{P} = [\mathbf{E}\{(b_n^{(1)})^*\mathbf{R}_n\} \cdots \mathbf{E}\{(b_n^{(m)})^*\mathbf{R}_n\} \cdots \mathbf{E}\{(b_n^{(M)})^*\mathbf{R}_n\}].$$

As usual, for a least squares implementation, the preceding expectations are replaced by empirical averages, with the estimation of $\mathcal{P}$ requiring a training sequence.

VI. Numerical Results

The performance of the proposed architecture is evaluated through simulations using the standard IEEE 802.11 mm-wave indoor channel model. Throughout the simulations, the OFDM symbol rate (or subband symbol rate) is $F_s = 256$ MHz and the carrier frequency is 60 GHz. Since the interference is encountered only from adjacent subbands, we consider a simulation scenario of three consecutive subbands ($M = 3$) and focus on the performance of the middle subband. The middle subband represents the full interference scenario since it receives interference from both the left and the right adjacent subbands. The mm-wave channel is generated using the conference room scenario as described in IEEE 802.11-09 for 60 GHz carrier frequency [6]. Throughout the simulations, we assume that the line of sight path is blocked and the transmitter and receivers are steered toward the strongest non-LOS path. We modeled the transmit and the receive filters, used in evaluating the baseband equivalent channels (5), (6), and (7), by the squared root raised cosine (SRRC) filter with excessive bandwidth of 12.5%.

The OFDM transmitter for each subband has 64 subcarriers ($N = 64$), with a cyclic prefix of 16 samples (the overhead due to the cyclic prefix can be reduced by increasing the number of subcarriers). Considering 256 MHz OFDM sampling rate, the channel spacing between subcarriers is 4 MHz (Table I) and we use 16-QAM modulation on each subcarrier. Channel coding is not considered, since our focus is on inter-band interference.

In Figure 7, we compare the bit error rate (BER) performance of a system with no interference suppression with a benchmark ISI-only system (i.e., only one subband is transmitted). The BER is averaged over 1000 independent realizations of the indoor conference room channel. Clearly, while OFDM with the given cyclic prefix is effective in dealing with the ISI of the beamformed channel, inter-band interference can significantly degrade performance (error floor of 3×10^{-2} after 20 dB SNR) unless suppressed. Figure 10 shows the BER v.s. OFDM subcarrier index for two specific SNR values (6 dB and 20 dB). We observe that if the interference suppression is not applied, as SNR increases, the BER decays except for boundary subcarriers. This confirms that the interference encountered from adjacent subbands appears only at the boundary subcarriers.

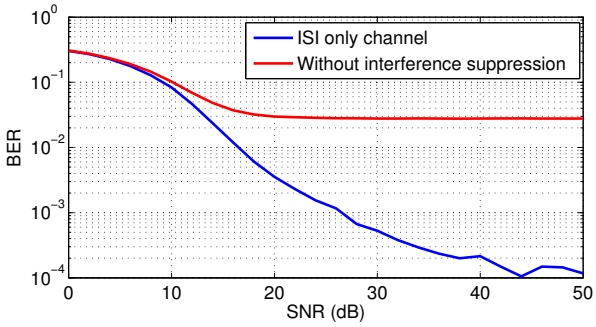

Fig. 7. Bit error rate (BER) vs. SNR for the middle subband with and without inter-band interference, averaged over 1000 independent channel realizations. No interference suppression is applied.

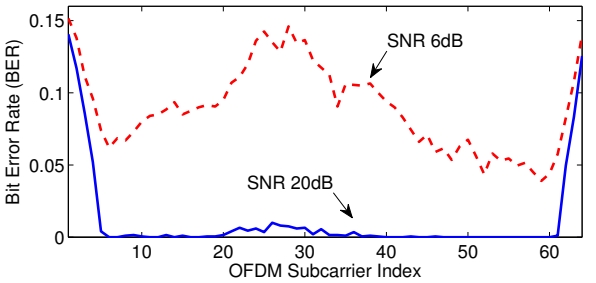

Fig. 8. Bit error rate (BER) vs. OFDM subcarrier for one realization of the channel when inter-band interference is not suppressed. BER decays with increasing SNR except for boundary subcarriers, which encounter interference from adjacent subbands.

Figure 9 shows BER performance vs. SNR when the ZF and MMSE linear equalizers are applied. For the ZF equalizer, we assumed that the channel state information for each subcarrier is known at the receiver. However, the MMSE linear equalizer is trained based on 50 OFDM training symbols. For the quasi-static indoor channels of interest, we expect that such training would be needed quite seldom (e.g., when starting up a link), with continuing adaptation in decision-directed mode. Even though we assume ideal channel estimation for the ZF equalizer, the penalty from noise enhancement is evident from Figure 9, where it is compared with the MMSE linear equalizer and the ISI-only benchmark. This is because we are using a relatively large 16QAM constellation, for which noise enhancement can severely impact performance even at moderately large SNRs. Figure 10 shows the amount of noise enhancement per subcarrier for the ZF equalizer. We observe that while the noise enhancement is negligible for the middle subcarriers, it is as large as 4 dB for the boundary subcarriers. However, in the overall system performance, the noise enhancement effect is not significant, since it only affects a few OFDM subcarriers.

In comparison with the ISI only scenario (Figure 7), we see that using a linear equalizer works well for interference

suppression and the performance results are close to that of the ISI-only benchmark. An error floor of 10^{-4} is also observed in the ISI-only benchmark, and is probably due to scenarios in which the length of the effective beamformed channel (desired or interfering) exceeds that of the cyclic prefix. This is borne out by Figure 11, which shows that the error floor falls to 10^{-5} when the cyclic prefix is increased from 16 to 20 samples.

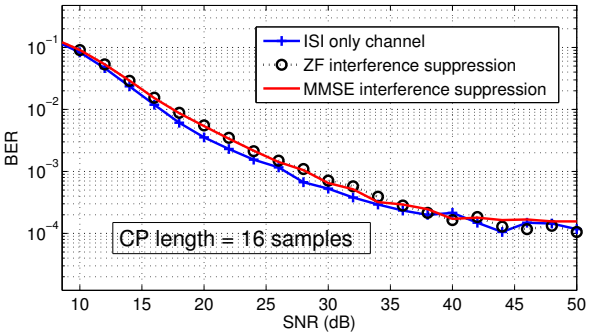

Fig. 9. BER vs. SNR when zero-forcing linear equalizer with known channel and MMSE equalizer with unknown channel are applied. The BER is averaged over 1000 independent channel scenarios and transmit data streams.

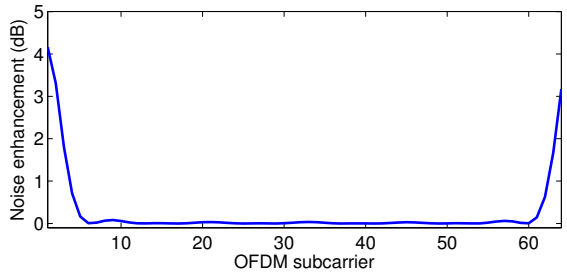

Fig. 10. The amount of noise enhancement for each subcarrier when zero-forcing linear equalizer is applied for inter-channel interference.

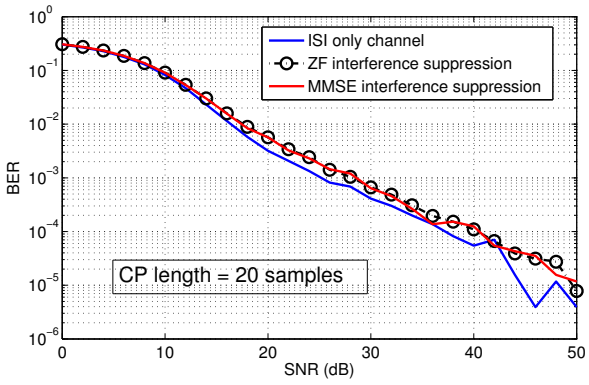

Fig. 11. The effect of increasing the CP length by 25% on system performance in comparison with Figure 9.

VII. Conclusions

Our results show that analog multiband with OFDM is an attractive option for very high rate communication over dispersive channels. For the indoor mm-wave communication system investigated here, linear MMSE adaptation is effective for suppressing the interference seen by the edge subcarriers. We view this work as only the first step in a comprehensive investigation of the potential for our approach for significantly increasing data rates, or reducing transceiver power consumption, relative to existing designs for IEEE 802.11ad. For the simple beamformed link considered here, it is important to develop coded modulation strategies potentially spanning multiple subbands for providing frequency diversity. We would also like to understand the source of the error floors. Are they because of the desired or the interfering subband's channel length exceeding the cyclic prefix, and is there some hybrid interference suppression/cancellation strategy for removing it? Of course, these error floors are low enough that they can be handled with light channel coding. An important topic for future work is the combination of diversity and multiplexing with beamforming (e.g., when there are multiple subarrays, each capable of beamforming independently) [9] in the context of analog multiband.

Acknowledgment

This research was supported in part by Samsung Research America - Dallas. We acknowledge the help and feedback from researchers in Samsung Research America - Dallas on this work.

References

[1] B. Murmann. ADC performance survey 1997-2014. [Online]. Available: http://www.stanford.edu/ murmann/adcsurvey.html.

[2] A. Amirkhany, V. Stojanovic, and M. Horowitz, "Multi-tone signaling for high-speed backplane electrical links," in *Proc. of the IEEE Globecom*, vol. 2, March 2004, pp. 1111–1117.

[3] A. Amirkhany, A. Abbasfar, J. Savoj, M. Jeeradit, B. Garlepp, R. Kollipara, V. Stojanovic, and M. Horowitz, "A 24 Gb/s software programmable analog multi-tone transmitter," *IEEE Journal of Solid-State Circuits*, vol. 43, no. 4, pp. 999–1009, February 2008.

[4] V. Dyadyuk, J. D. Bunton, J. Pathikulangara, R. Kendall, O. Sevimli, L. Stokes, and D. A. Abbott, "A multigigabit millimeter-wave communication system with improved spectral efficiency," *IEEE Trans. on Microwave Theory and Techniques*, vol. 55, no. 12, pp. 2813–2821, December 2007.

[5] H. Zhang, S. Venkateswaran, and U. Madhow, "Analog multitone with interference suppression: Relieving the ADC bottleneck for wideband 60 GHz systems," in *Proc. of the IEEE Globecom*, 2012, pp. 2305–2310.

[6] "Channel models for 60 GHz WLAN systems," *IEEE 802.11-09/0334r8*, 2010.

[7] A. Maltsev, R. Maslennikov, A. Lomayev, A. Sevastyanov, and A. Khoryaev, "Statistical channel model for 60 GHz WLAN systems in conference room environment," *Radioengineering*, vol. 20, no. 2, pp. 409–422, June 2011.

[8] H. Xu, V. Kukshya, and T. S. Rappaport, "Spatial and temporal characteristics of 60 GHz indoor channels," *IEEE Journal of Selected Areas in Communications*, vol. 20, no. 3, pp. 620–630, April 2002.

[9] E. Torkildson, U. Madhow, and M. Rodwell, "Indoor millimeter wave MIMO: Feasibility and performance," *IEEE Transactions on Wireless Communications*, vol. 10, no. 12, pp. 4150–4160, December 2011.